Antibacterial effects of titanium embedded with silver nanoparticles based on electron-transfer-induced reactive oxygen species

CrossMark

Guomin Wang [a], Weihong Jin [a], Abdul Mateen Qasim [a], Ang Gao [a], Xiang Peng [a], Wan Li [a], Hongqing Feng [a, b, **], Paul K. Chu [a, *]

[a] Department of Physics and Materials Science, City University of Hong Kong, Tat Chee Avenue, Kowloon, Hong Kong, China
[b] Beijing Institute of Nanoenergy and Nanosystems, Chinese Academy of Sciences; National Center for Nanoscience and Technology (NCNST), Beijing 100083, PR China

A R T I C L E   I N F O

A B S T R A C T

Although titanium embedded with silver nanoparticles (Ag-NPs@Ti) are suitable for biomedical implants because of the good cytocompatibility and antibacterial characteristics, the exact antibacterial mechanism is not well understood. In the present work, the antibacterial mechanisms of Ag-NPs@Ti prepared by plasma immersion ion implantation (PIII) are explored in details. The antibacterial effects of the Ag-NPs depend on the conductivity of the substrate revealing the importance of electron transfer in the antibacterial process. In addition, electron transfer between the Ag-NPs and titanium substrate produces bursts of reactive oxygen species (ROS) in both the bacteria cells and culture medium. ROS leads to bacteria death by inducing intracellular oxidation, membrane potential variation, and cellular contents release and the antibacterial ability of Ag-NPs@Ti is inhibited appreciably after adding ROS scavengers. Even though ROS signals are detected from osteoblasts cultured on Ag-NPs@Ti, the cell compatibility is not impaired. This electron-transfer-based antibacterial process which produces ROS provides insights into the design of biomaterials with both antibacterial properties and cytocompatibility.

© 2017 Elsevier Ltd. All rights reserved.

1. Introduction

Although titanium and titanium alloys with good stability and biocompatibility in the physiological environment are widely used in dental and orthopedic implants [1—3], the materials do not have intrinsic antibacterial ability. Bacterial infection is one of the most serious complications after surgery leading to not only implant failure, but also complication, morbidity, and mortality [4—6]. Several strategies have been proposed to endow titanium implants with antibacterial characteristics. In particular, titanium embedded with silver nanoparticles (Ag-NPs@Ti) by plasma ion immersion implantation (PIII) has drawn much attention because of the broad antibacterial spectrum and capability of tuning the surface

morphology of the biomaterials [7,8]. However, the exact antibacterial mechanism of Ag-NPs@Ti is still not well understood.

The antibacterial mechanism of Ag-NPs in liquids have been investigated. Sondi et al. assumed that accumulation of Ag-NPs on the cell wall and bacteria membrane increased the permeability leading to cell death [9]. Free silver radicals were detected from the bacteria solution after treating with Ag-NPs [10] and the cell metabolism was disrupted by Ag^+ leached from the Ag-NPs [11—13]. However, the Ag-NPs embedded in the substrate are different from those dispersed in liquids because of interactions with both the substrate and bacteria in physiological liquids upon contact. The micro-galvanic effects between Ag and titanium evoke electron transfer in the surrounding medium and in fact, electron transfer is a universal behavior in bacteria and cell respiration. However, there have been few studies on the effects by considering both the materials and biological aspects and concomitant interactions between the biomaterials and biological system. What's more, whether reactive oxygen species (ROS) is produced or not is a fundamental issue in antibacterial processes. There have been recent studies on the role of ROS in antibacterial processes suggesting practical approaches to enhance our current antibiotics

---

* Corresponding author. Department of Physics and Materials Science, City University of Hong Kong, Tat Chee Avenue, Kowloon, Hong Kong, China.
** Corresponding author. Beijing Institute of Nanoenergy and Nanosystems, Chinese Academy of Sciences; National Center for Nanoscience and Technology (NCNST), Beijing 100083, PR China.
E-mail addresses: fenghongqing@binn.cas.cn (H. Feng), paul.chu@cityu.edu.hk (P.K. Chu).

arsenal [14–16]. In fact, Nathan et al. have suggested that a better understanding of how to manipulate ROS production can spur medical advances in immunology and combination therapy [17]. Thus, as potential bone implant materials, it is important to study whether Ag-NPs@Ti induces ROS during bacteria killing and a better understanding will aid the design and fabrication of future biomaterials.

In this work, Ag-NPs are incorporated into titanium by PIII and the antibacterial characteristics and mechanism are investigated. The antibacterial effect of Ag-NPs on different substrates is determined. Our results show that electron transfer between the Ag-NPs and titanium produces a large amount of ROS which play a key role in bacteria killing by inducing physiological changes in the bacteria such as intracellular oxidation, protein and DNA/RNA release, as well as membrane potential variation.

2. Experimental section

2.1. Sample preparation and characterization

2.1.1. Sample preparation

Titanium (Ti, 99.99%) samples with dimensions of 10 mm × 10 mm × 1 mm were ground with SiC abrasive paper (from 400 grit to 2000 grit), mounted on a sample holder, introduced into a plasma immersion ion implanter, and evacuated to a base pressure of 2.5×10^{-3} Pa. Ag (99.99%) produced by a filtered cathodic arc plasma source was implanted into the polished Ti samples which were pulse-biased to −30 kV (pulse duration of 450 μs and frequency of 6 Hz). The samples were plasma-implanted for 1 h, 2 h, or 3 h (samples designated as 1 h-Ag-NPs@Ti, 2 h-Ag-NPs@Ti, and 3 h-Ag-NPs@Ti, respectively). More details about the PIII process can be found elsewhere [8].

2.1.2. Surface characterization

Atomic force microscopy (AFM, Veeco's MultimodeV, Veeco, USA) and scanning electron microscopy (SEM, JSM 7001F, JEOL, Japan) were conducted to characterize the surface morphology. The X-ray diffraction (XRD) spectra were acquired on a Philips Siemens D500 X-ray diffractometer and X-ray photoelectron spectroscopy (XPS, K-Alpha, Thermo Fisher Scientific, USA) was conducted to determine the chemical states (sputtering rate of about 7 nm/min). Energy dispersive X-ray spectroscopy (EDS) on the SEM were used to determine the silver concentration. The experimental procedures are illustrated schematically in Fig. S1.

2.1.3. Electrochemical measurements

The electrochemical properties of the samples were determined on an electrochemical workstation (Zennium, Zahner, Germany) using a three-electrode configuration comprising a saturated calomel electrode (SCE) as the reference electrode, a platinum rod as the counter electrode, and the sample (area of 0.5 cm^2) as the working electrode. The electrochemical measurements were performed at room temperature. The open circuit potential (OCP) measurements were carried out before the Tafel curves were acquired at a scanning rate of 1 mV/s from −0.5 V to 0.5 V with respect to OCP.

2.2. Antibacterial effects

2.2.1. Antibacterial effects of Ag-NPs@Ti

Four groups of samples, namely Ti with 0.1 mM H_2O_2 (ROS positive group), 1 h-Ag-NPs@Ti, 2 h-Ag-NPs@Ti, and 3 h-Ag-NPs@Ti, and the unprocessed Ti control were studied. The samples were immersed in 75% ethanol for 15 min and dried in a biosafety cabinet. Afterwards, each sample was put on the well of a 24-well plate and the biofilm forming strains of Staphylococcus aureus (ATCC 29213) and Escherichia coli (ATCC 25922) were introduced. S. aureus and E. coli were cultured in the Lysogeny broth (LB) medium overnight at 37 °C in an incubator shaken at 220 rpm. The bacteria solution was diluted to $OD_{600} = 0.1$ with the fresh medium and cultivated for another 3 h for reactivation. The bacteria solution was diluted to a concentration of $2-3 \times 10^5$ CFU/mL and 100 μL were spread on the surface of the samples. The gaps between the wells were filled with autoclaved water in order to prevent evaporation of the medium. At time points of 1, 3, 6, 18 and 24 h, the adhered bacteria were detached from the surface with 900 μL of phosphate buffered saline (PBS), diluted to the proper concentration, spread on a solid agar plate, and cultivated for another 16 h to count the colony forming unit (CFU). The antibacterial rate was determined by the following formula:

$$\text{Antibacterial rate} = \left(1 - \frac{\text{CFU}_{\text{experimental group}}}{\text{CFU}_{\text{control group}}}\right) \times 100\%$$

2.2.2. Antibacterial effects of Ag-NPs on different substrates

The antibacterial effect of 2 h-Ag-NPs on substrates with different conductivity, namely Ti (conductor), Si (semiconductor), and SiO_2 (insulator) was assessed. Based on the antibacterial results of Ag-NPs@Ti, an incubation time of 6 h was chosen and CFU counting was performed to compare the antibacterial rates according to session 2.2.1 above.

2.2.3. Live/dead staining

In the viability assay, after rinsing in PBS twice for 5 min, the sample with bacteria was stained with LIVE/DEAD® Baclight Bacterial Viability Kit (L7007, Invitrogen, USA) for 15 min in darkness. The samples were then examined on an inverted microscope (BM-20AYC, BM) with 420–480 nm and 520–580 nm as the excitation and emission wavelengths (green fluorescence) and 480–550 nm and 590–800 nm as the excitation and emission wavelengths (red fluorescence). Representative images were obtained and merged.

2.3. Intracellular oxidative stress measurement

2.3.1. Intracellular ROS level evaluation

The intracellular ROS level was investigated by fluorescence imaging. At time points of 1, 3, 6, 18, and 24 h, the samples were washed with PBS twice and 100 μL of 2′, 7'-dichlorodihydro-fluorescein diacetate (DCFH-DA, Beyotime, China) were added to the surface and reacted for 15 min. The excess dye was washed with PBS and the samples were observed by inverted fluorescent microscopy as mentioned above. Flow cytometry (FCM, BD FACS Calibur, USA) was employed to determine quantitatively the intracellular ROS level using 488 nm and 522 nm as the excitation and emission wavelengths. The X Geo mean data of FL1-H was used to evaluate the fluorescence intensity of each group.

2.3.2. Intracellular superoxide concentration detection

The intracellular superoxide was quantitatively measured with the Superoxide Assay Kit (S0060, Beyotime, China) to evaluate the intracellular oxidative stress level after culturing for 3 and 6 h. The bacteria solution was collected and diluted to a proper concentration before the assay kit was added. After cultivation for another 3 min at 37 °C, OD_{450} and OD_{600} were monitored to quantitatively determine the superoxide.

2.3.3. Protection effect of antioxidant

To confirm the oxidative stress rendered by Ag-NPs@Ti, N-

acetylcysteine (NAC, sigma, USA) was used as the antioxidant to protect the bacteria from oxidative damage [18]. NAC was added to the bacteria solution (10 mM and 50 mM) and 100 μL were spread on the samples surface and cultivated for 24 h. Afterwards, the adhered cells were collected and spread on an agar plate and the CFU was determined 16 h later.

2.3.4. Intracellular components leakage and membrane potential test

The leakage of intracellular compounds reflects the permeability of the cell membrane and cell wall [19]. The BCA protein assay kit (Sigma, US) was used to determine the extracellular protein concentration of the bacteria suspension and the detailed process could be found elsewhere [20]. The released DNA/RNA was estimated by measuring the absorbance at 260 nm on a NanoDrop spectrophotometer (ND-1000, Thermo Fisher Scientific, USA).

The *Bac*Light™ Bacterial Membrane Potential Kit (B34950, Invitrogen, USA) was used to monitor the membrane potential change of the bacteria cultivated on different samples for different time durations. As CCCP (carbonyl cyanide *m*-chlorophenyl hydrazone) could decrease the membrane potential, *S. aureus* treated with CCCP served as the positive group while the untreated *S. aureus* was the negative control group. To stain the bacteria, 10 μL of DiOC$_2$(3) (3,3'-diethyloxacarbocyanine Iodide, 3 mM) were added to 990 μL of *S. aureus* and cultivated for 15 min in darkness. Subsequently, 500 μL of the stained bacteria solution were assayed by FCM. An excitation wavelength of 488 nm was used to excite DiOC$_2$(3) and the green and red fluorescence was simultaneously detected using 530 nm and 610 nm band-pass filters, respectively. The degree of membrane depolarization was characterized by the red/green fluorescence ratio and more detailed information about the procedures were described in a previous study [21].

2.4. Physiochemical characterization of the culture medium before and after treatment

The oxidation-reduction potential (ORP) and pH were determined during the 24 h culturing period with an ORP probe (Clean L'eau ORP30, USA) and pH probe (Clean L'eau PH30, USA) following the protocols in previous studies [22]. The concentration of released Ag$^+$ was also determined. Each sample was immersed in 1 mL of PBS at 37 °C and the solution was collected 24 h later. Fresh PBS was added to the remaining sample and after 24 h, the solution was collected. The concentration of Ag$^+$ in the solutions was determined by inductively-coupled plasma mass spectroscopy (ICP-MS, Agilent 7500, Agilent, US).

2.5. Oxidative stress of Ag-NPs@Ti on MC3T3-E1 osteoblasts

The MC3T3-E1 osteoblasts purchased from the cell bank of the Chinese Academy of Sciences were used to study the biocompatibility of Ag-NPs@Ti. The cells were cultured in dulbecco's modified eagle medium (DMEM) containing 10% fetal bovine serum (FBS) on 90 mm petri dishes and incubated at 37 °C under 5% CO$_2$. The culture medium was replaced with the fresh medium every other day. To monitor cell adhesion and cytotoxicity, the cells in the logarithmic growth phase were harvested, centrifuged for 5 min, and adjusted to a density of 2×10^4 cells/mL with the fresh medium before 1 mL of the cell solution was seeded on the disinfected sample on a 24-well plate. To assess adhesion, the cells were rinsed with PBS twice, fixed with 4% paraformaldehyde, permeabilized with 0.2% Triton X-100 (sigma, USA), stained with phalloidin-fluorescein isothiocyanate (Sigma, USA) for 60 min, and then stained with 4′,6-diamidino-2-phenylindole (DAPI, sigma, USA) for 5 min. The samples were observed under an inverted microscope

(20AYC-BM, BM). The 3-(4,5-dimethylthiazol-2-yl)-2,5-diphenyl tetrazolium bromide (MTT) assay was employed to evaluate the cell proliferation and viability. At time points of 24, 72, and 120 h, the medium on the 24-well plate was replaced with the MTT solution and cultivated for 4 h. Afterwards, the MTT solution was replaced with the DMSO solution to dissolve formazan crystals. 100 μL of the solution were transferred to a 96-well plate and measured on a multimode reader (BioTek, US) at an excitation wavelength of 570 nm. The wells with DMSO served as the negative control group. To estimate the intracellular ROS levels, the cells were cultivated on the samples on a 24-well plate. After 4 and 24 h, the cells were rinsed with PBS twice and treated with DCFH-DA and DAPI for 30 min at 37 °C as described previously [23]. The samples with adhered cells were rinsed with PBS and examined by inverted fluorescent microscopy. The blue nuclei represented cells adhered to the surface and green fluorescence represented cells with positive ROS signals.

2.6. Statistical analysis

Each experiment was repeated at least 3 times and the results were shown as mean ± stand deviation (SD) and analyzed by Student *t*-test and ANOVA test. A value of $p < 0.05$ was considered statistically significant.

3. Results

3.1. Characterization of samples

The detailed morphology of the samples obtained by AFM is exhibited in Fig. 1a—d. The small Ag-NPs are distributed evenly on the titanium plate after PIII for 1 h and the Ag-NPs become larger after PIII for 2 h—3 h. The particles in 3 h-Ag-NPs@Ti are more than two times bigger than those in 2 h-Ag-NPs@Ti. The roughness of 1 h-Ag-NPs@Ti is the smallest and increases with implantation time (Fig. 1e). Some plasma etching effects are observed from 1 h-Ag-NPs@Ti [24]. When the ion implantation time is increased, larger NPs form thus increasing the surface roughness. The SEM images (Fig. 1f—i) are consistent with the AFM images showing that the size of the Ag-NPs increases with PIII time. Although only Ti peaks can be found from the XRD patterns (Fig. S2), obvious Ag peaks emerge from the full XPS spectra of the Ag-NPs@Ti samples (Fig. 1j) suggesting limited implantation depth and amount of Ag. The Ag concentration is determined by XPS (Fig. 1k—m) and the maximum implantation depth of Ag in the three samples is about 80 nm. The amount of Ag increases as the PIII time goes up from 1 h to 3 h being consistent with the quantitative EDS result (Fig. 1n). The corrosion information can be obtained from the polarization curves (Fig. 1o). The corrosion potentials (E$_{cor}$) of Ti and 1 h-, 2 h-, and 3 h-Ag-NPs@Ti are −0.207 V, −0.177 V, −0.207 V and −0.216 V, respectively and the difference is quite small. However, the corrosion current (I$_{cor}$) increases as the ion implantation time is increased from 1 h to 3 h thus more easily activating the microgalvanic couples and triggering electron transfer [8].

3.2. Antibacterial properties

As shown in Fig. 2a and b, the antibacterial rates of the four groups against *S. aureus* and *E. coli* increase during culturing for 24 h. 2 h-Ag-NPs@Ti shows antibacterial rates of 90% against *S. aureus* and 99% against *E. coli* at the 24 h time point and they are the best among the three Ag-NPs@Ti groups. The trend is similar to the antibacterial effect observed from 0.1 mM H$_2$O$_2$. The antibacterial rate of 1 h-Ag-NPs@Ti is the smallest in the beginning but reaches the same level as 3 h-Ag-NPs@Ti a few hours later.
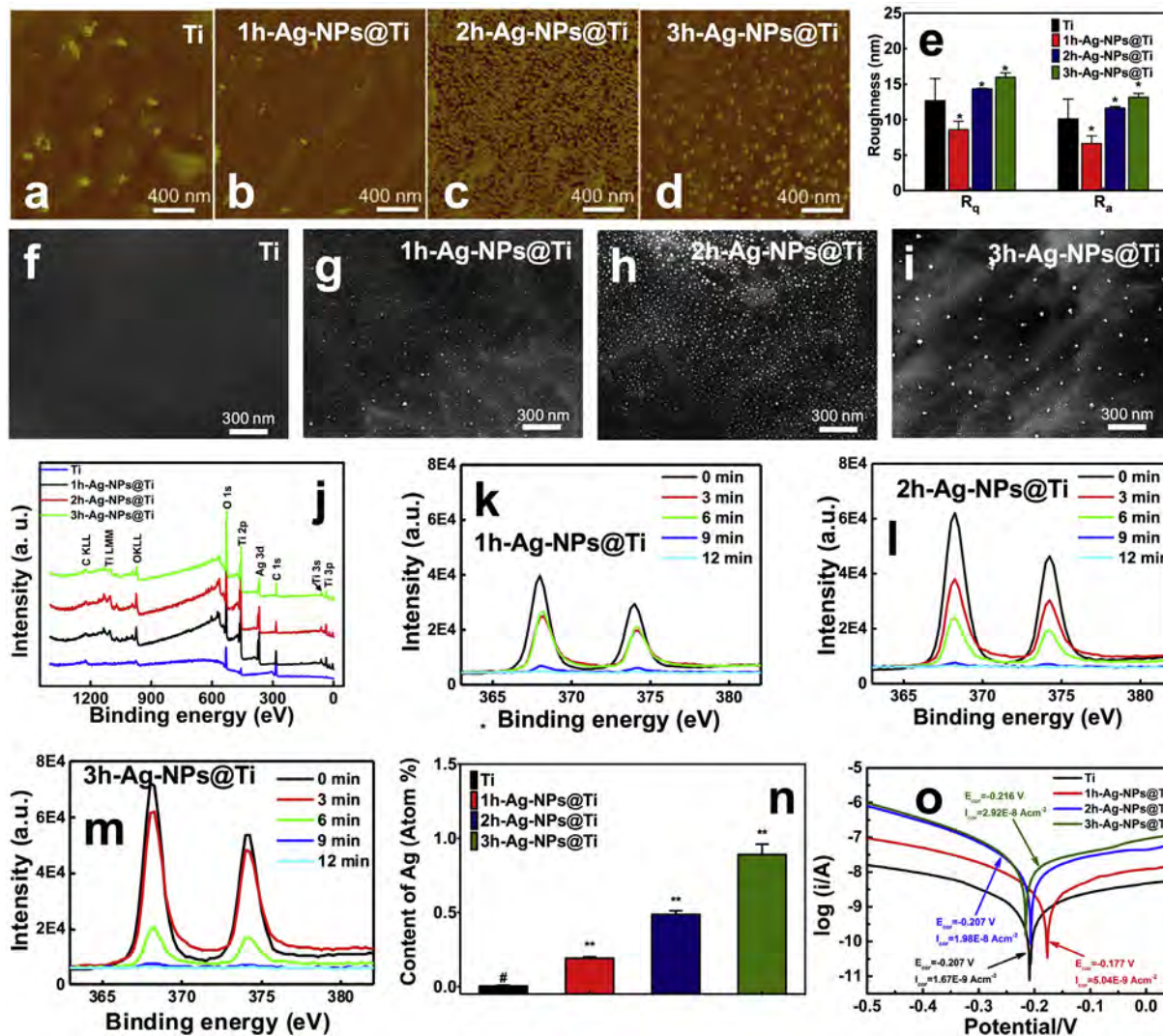
Fig. 1. Sample characteristics: Surface morphology observation by AFM (a—d) and SEM (f—i). (e) Surface roughness of samples. R_a means arithmatic average of the absolute value and R_q is the root mean square. (j) XPS full spectrum of samples. (k—m) high-resolution spectra of Ag 3d acquired by XPS. (n) Content of Ag (Atom %) in samples got by EDS in SEM. # denotes an absolutely negative result. (o) Polarization curves of samples with the E_{cor} and I_{cor} of each group marked. * denotes $p < 0.05$ when compared to the Ti group.

Comparing the two strains of bacteria, *E. coli* shows higher sensitivity to Ag-NPs@Ti than *S. aureus*. It can be explained by the thicker membrane on Gram-positive bacteria [25]. Consequently, the stronger *S. aureus* is selected in our subsequent study of the antibacterial mechanism. The morphology of *S. aureus* proliferating on the samples is examined by SEM (Fig. S3) and smaller bacteria numbers are observed being consistent with the CFU counting results.

3.3. Influence of substrates on the antibacterial properties

The antibacterial ability of the implanted 2 h-Ag-NPs in Ti (conductor), Si (semiconductor), and SiO₂ (insulator) is evaluated. After culturing for 6 h, the antibacterial effects are different as shown in Fig. 2c. The antibacterial effects are more pronounced on Ag-NPs@Ti than Ag-NPs@Si and Ag-NPs@SiO₂, suggesting that a conducting substrate is essential to inhibition of bacteria growth. In a conductor, electrons flow freely from particles to particles and free electrons can arrive at Ag-NPs embedded in Ti readily. The larger I_{cor} observed from the Tafel curve (Fig. 1o) further demonstrates that the embedded Ag-NPs enhance the electron transfer

process during immersed in the solution and the micro-galvanic couples between Ti substrate and Ag-NPs can be activated easily. By taking into account the micro-galvanic effects between the Ag-NPs and Ti substrate, it is likely that electron transfer between the Ag-NPs and substrate influences the bacteria leading to bacteria death.

3.4. Oxidative stress study on bacteria

3.4.1. Intracellular ROS

Because the antibacterial curve of 2 h-Ag-NPs@Ti is almost the same as that of 0.1 mM H₂O₂, the intracellular ROS is stained simultaneously with bacteria viability staining to determine whether ROS is involved in the bacteria killing process (Fig. 3). When cultivated on the Ti plate, the bacteria proliferate nicely and cover the sample surface and the ROS signal is negative during the 24 h cultivation time. However, the situation is different for the bacteria in the Ag-NPs@Ti groups. The density of *S. aureus* increases significantly from 3 h to 6 h and large numbers of bacteria cells with strong intracellular ROS signals are detected at 3 h and 6 h as well. Afterwards, the number of ROS positive cells decreases together
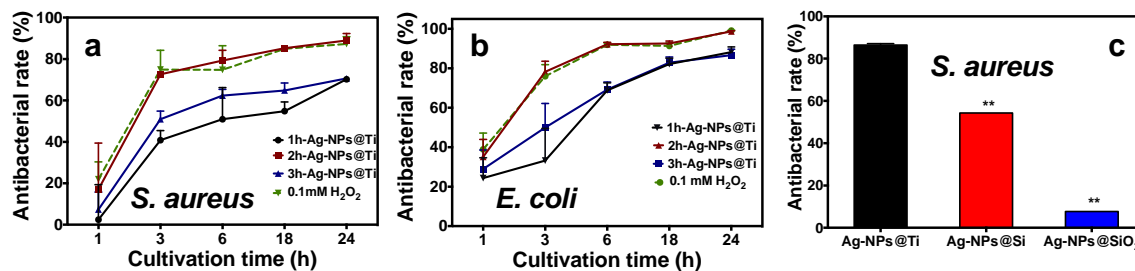
Fig. 2. Antibacterial rates of the Ag-implanted samples: (a, b) Antibacterial rate of Ag-NPs@Ti with different implantation durations on *S. aureus* and *E. coli,* respectively. (c) 6 h antibacterial rates of Ag-NPs on substrates with different conductivity. ** denotes $p < 0.01$ compared to Ag-NPs@Ti group.

with the drop in the live cell density on the Ag-NPs@Ti samples. When the culture time is prolonged to 24 h, scattered ROS positive spots can still be detected from the three Ag-NPs@Ti groups.

The ROS level of the bacteria cultured on the samples for 3 h and 6 h is determined quantitatively by FCM based on fluorescence staining (Fig. 4a). More ROS signal is detected from the solution with a larger H_2O_2 concentration and they are significantly different from the negative signals observed from the control group. The bacteria treated with 0.1 mM H_2O_2 show a similar ROS level as those treated with 2 h-Ag-NPs@Ti, which is the strongest among the three Ag-NPs@Ti groups. These results verify that Ag-NPs@Ti induces intracellular ROS in bacteria and it should be responsible for the antibacterial effect.

3.4.2. Intracellular superoxide

The intracellular superoxide is quantitatively measured and the results are displayed in Fig. 4b. OD_{450} reflects the intracellular superoxide level and a larger H_2O_2 concentration increases the intracellular superoxide in *S. aureus*. The superoxide levels in the three Ag-NPs@Ti groups and 0.1 mM H_2O_2 group show little difference ($p > 0.05$), although they are significantly larger than that in the control group ($p < 0.05$).

3.4.3. Protection effect of antioxidant

To further investigate the antibacterial effects of oxidative stress, NAC with two concentrations is introduced as the antioxidant and the antibacterial rate is determined again (Fig. 4c). NAC itself has little impact on bacteria growth. When the bacteria solution containing 10 mM NAC is cultivated on Ag-NPs@Ti, the antibacterial rate decreases significantly. When the concentration of NAC is increased to 50 mM, the antibacterial ability of Ag-NPs@Ti and H_2O_2 is almost completely inhibited. The results suggest that the Ag-NPs on Ti induce intracellular ROS production on *S. aureus* and this is a key reason for the antibacterial effect.

3.4.4. Physiological changes caused by ROS

The concentration of leaked proteins and DNA/RNA as well as the membrane potential are monitored to study the physiological properties of *S. aureus* before and after the treatment. Compared to the control group, the concentrations of leaked proteins of the three Ag-NPs@Ti groups are larger when the culture time is extended from 1 h to 6 h and a similar trend is observed from the H_2O_2 groups as shown in Fig. 5a. On the other hand, the concentrations of leaked DNA/RNA of the Ag-NPs@Ti groups are the same and they are also larger than those of the control groups but similar to those of the 0.1 mM H_2O_2 group as shown in Fig. 5b. In the determination of the membrane potential by monitoring the red/green fluorescence intensity ratio, the membrane potentials of the three Ag-NPs@Ti groups are between the levels of the CCCP positive and control groups but are similar to those of the 0.1 mM H_2O_2 groups as shown in Fig. 5c.

3.5. ORP/pH and Ag$^+$ concentration monitoring of the culture medium on the samples

The above results provide clue that electron transfer between the implanted Ag-NPs and Ti substrate induces strong intracellular ROS which plays an important role in bacteria killing. It has been reported that electron transfer produces a H$^+$ depletion region which can cause bacteria death [8]. Release of Ag$^+$ from the Ag-NPs may also disturb cell metabolism [9,10,26]. To discern their roles, the ORP, pH change, and Ag$^+$ concentration of the pure culture medium without bacteria are monitored. The ORPs in each group increase obviously during the 24 h culture time except the H_2O_2 group which shows a constant trend. The ORP of the 2 h-Ag-NPs@Ti group is the largest among the Ag-NPs@Ti groups reaching the same value as that of the 0.1 mM H_2O_2 group after 6 h ($p > 0.05$). The ORPs of the Ag-NPs@Ti groups are all significantly larger than those of the control group and the difference becomes larger indicating higher oxidative stress in the Ag-NPs@Ti groups (Fig. 6a). The pH of the Ag-NPs@Ti groups are lower than that of the 0.1 mM H_2O_2 group and control group after 18 h (Fig. 6b), which is different from the inference of the previous results of Cao et al. [8]. The final pH is 6.8−7.0 which is still physiologically suitable for *S. aureus* [27]. The concentration of released Ag$^+$ is less than 5 ppb (Fig. 6c) and such a low concentration should not pose any threat to bacteria. These results demonstrate that the interactions between the Ag-NPs and Ti produce a large amount of ROS, but not big changes in the pH or Ag$^+$. Our results supply evidence bacteria are killed by the strong oxidative stress rather than pH change or Ag$^+$ for Ag-NPs@Ti.

3.6. Oxidative stress in MC3T3-E1 osteoblasts on Ag-NPs@Ti

The compatibility of Ag-NPs@Ti with bone cells is evaluated and Fig. 7a−d show the MC3T3-E1 osteoblasts on the samples. The cells in the four groups all start to adhere after 4 h and those on 1 h-Ag-NPs@Ti and 2 h-Ag-NPs@Ti spread better than those on Ti and 3 h-Ag-NPs@Ti. After 20 h, the cells on 1 h-Ag-NPs@Ti and 2 h-Ag-NPs@Ti grow better than those on Ti group and 3 h-Ag-NPs@Ti. Cell proliferation is studied by the MTT test (Fig. 7e). Similar to cell adhesion, cell proliferation in the 1 h-Ag-NPs@Ti group is the highest and significantly higher than that of the control group. 2 h-Ag-NPs@Ti shows no appreciable difference compared to the Ti control. 3 h-Ag-NPs@Ti is slightly lower than the Ti control after 5 days ($p < 0.05$).

ROS imaging and DAPI staining (Fig. 7f) show obvious intracellular ROS signal after 4 h for the three Ag-NPs@Ti groups, which is similar to the 0.1 mM H_2O_2 group. After culturing for 24 h, the intracellular ROS signal becomes weak but is still detectable, suggesting that similar to the interactions between Ag-NPs@Ti and bacteria, Ag-NPs@Ti can also induce the production of intracellular ROS on osteoblasts, but the ROS does not have adverse effect on
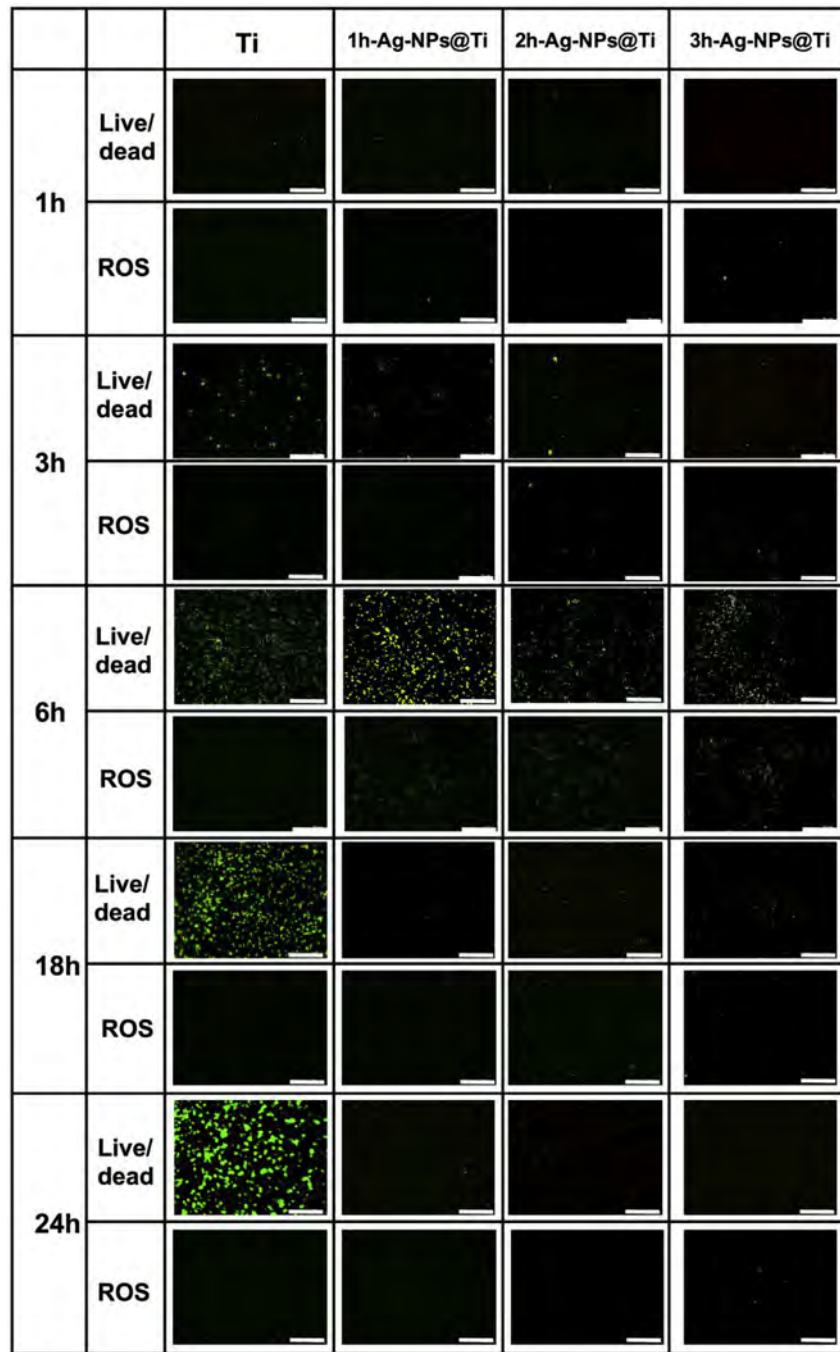
Fig. 3. Live/dead staining and intracellular ROS staining results at different cultivation time points. The scale bar is 50 μm.

osteoblast growth when the implantation time is less than 2 h.

4. Discussion

As a non-specific biocidal agent effective against a broad spectrum of bacteria, silver has been investigated extensively. However, the commonly fabricated mobile Ag NPs are usually not stable and can aggregate in solutions and introduction of detergents or stabilizers affects the toxicity of the NPs [28,29]. Ag-NPs@Ti fabricated by PIII has good antibacterial activity, biocompatibility, safety, and stability than traditional mobile Ag-NPs thus avoiding aggregation or toxicity mentioned above. Boasting desirable properties and

potential clinical application, Ag-NPs@Ti prepared by PIII is an excellent candidate for the investigation of antibacterial mechanisms. However, many studies so far have mainly focused on the level of antibacterial activity but do not assess in details the physiological changes in the bacteria induced by the biomaterials.

In this work, the antibacterial activity of Ag-NPs@Ti is explored systematically. The highest antibacterial activity observed from 2 h-Ag-NP@Ti can be explained as follows. First of all, the size and dose of the Ag-NPs influence the antibacterial effects [30]. Morones et al. found that only silver particles with diameters of 1—10 nm could interact with bacteria [12] and Cao reported that the antibacterial activity of smaller Ag-NPs (4 nm in diameter) was inferior to that of
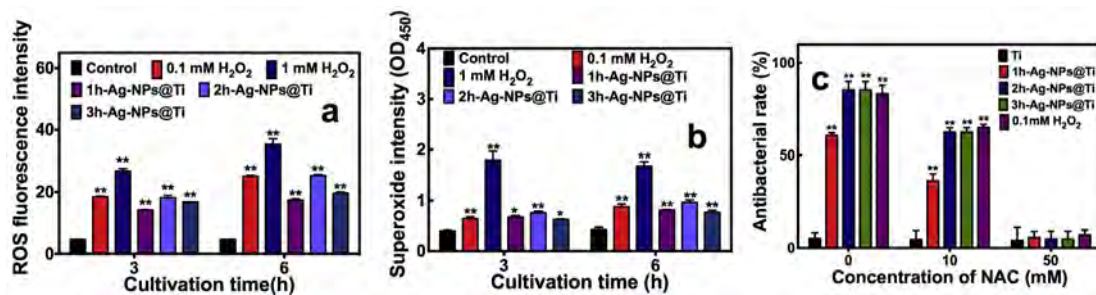
Fig. 4. Oxidative stress evaluation: (a) Quantitative analysis of intracellular ROS with FCM based on fluorescent staining. (b) Intracellular superoxide levels in the Ag-NPs@Ti groups with comparison to control group and H_2O_2 groups. (c) Antibacterial rates of the samples under protection by the antioxidant (NAC). * means $p < 0.05$ and **means $p < 0.01$ compared to the control group.
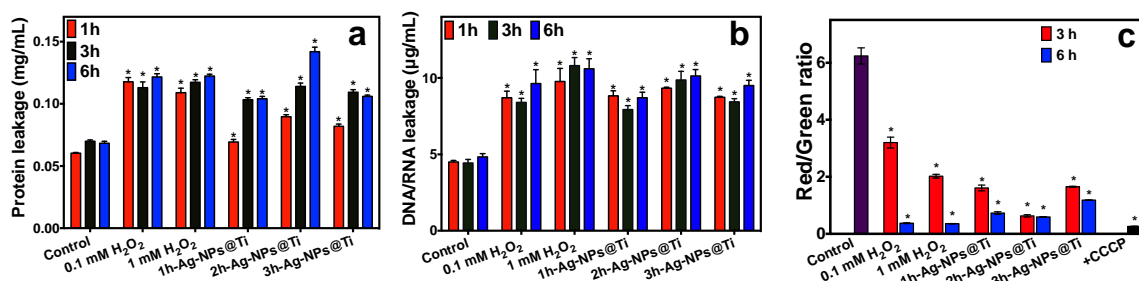

Fig. 5. Bacteria membrane integrity evaluation showing the concentration of leaked (a) protein and (b) DNA/RNA compared to the negative group and H_2O_2 groups. (c) Membrane potential of Ag-NPs@Ti groups with comparison to control group and H_2O_2 groups. A higher red/green fluorescence intensity ratio means a higher membrane potential. * Denotes a significant difference compared to the Ti group ($p < 0.05$).
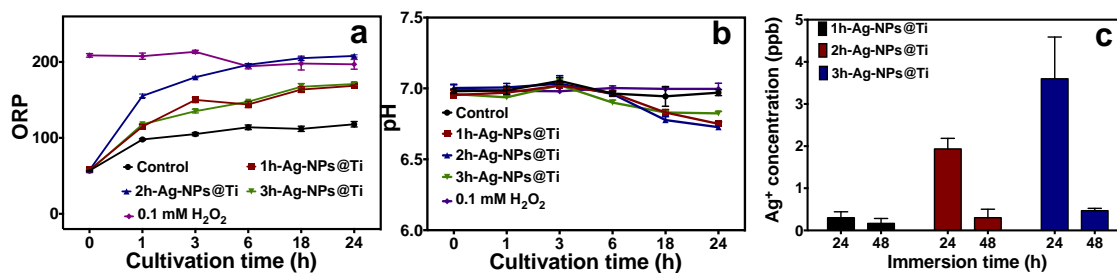

Fig. 6. Physiochemical characterization of the bacteria solutions before and after treatment: (a) ORP change in the culture medium for different surfaces. The ORPs of the control group are significantly lower than those of the Ag-NPs@Ti and 0.1 mM H_2O_2 groups at 1 h, 3 h, 6 h, 18 h, and 24 h ($p < 0.05$). (b) pH of the bacteria solution during the 24 h culturing time. The pHs of the control group are significantly higher than that of the Ag NPs@Ti groups at time points of 18 h and 24 h ($p < 0.05$). (c) Concentration of Ag$^+$ released from Ag-NPs@Ti for 48 h.

large Ag-NPs (5−25 nm in diameter) [31]. As the diameters of 1 h-, 2 h- and 3 h-AgNPs@Ti in this study are ~4 nm, ~10 nm and ~40 nm, respectively, 2 h-Ag-NPs@Ti is supposed to have better interactions with bacteria. On the other hand, 2 h-Ag-NPs@Ti has a larger density of NPs, and the larger contact area also contributes to a higher antibacterial rate. In addition, as a rougher surface favors adhesion of *S. aureus* [32,33], the smaller roughness of 2 h-Ag-NPs@Ti is another reason for the higher antibacterial rate compared to 3 h-Ag-NPs@Ti.

Our results demonstrate that the electrical conductivity of the substrate is very important to bacteria inactivation. Our observation is consistent with a previous study on graphene that a conducting substrate endows graphene with antibacterial properties but an insulating one does not, thereby suggesting the importance of charge in the antibacterial process [34]. Micro-galvanic couples are formed between the embedded Ag-NPs and the Ti substrate because of the different standard electrode potentials. During

immersion in a solution, as the standard electrode potential of Ti is 2.4 V more negative than that of Ag [35], Ti is oxidized to Ti^{n+} [Equation (1)] by losing electrons which can be transferred to Ag with ions in the near surface moving in the specific direction to produce the micro-galvanic effects. Cao et al. have suggested that bacteria are killed because of H$^+$ depletion during which H$^+$ is consumed to produce OH$^-$ [8]. However, our results are somewhat different. While the pH of the control group is unchanged, that of the Ag-NPs @Ti surface decreases gradually from 7.0 to 6.8, which can in fact be well adapted by *S. aureus* to offset the possibility of H$^+$ depletion [36,37]. In our following experiments, the Ag-NPs@Ti groups show larger ORP levels than the control group. The ORP of the 2 h-Ag@Ti group reaches the same level as that of the 0.1 H_2O_2 group after 6 h. Therefore, the bacteria do not appear to die from H$^+$ depletion, but rather oxidative stress. The electrons donated by Ti are not consumed to form H_2, OH$^-$, or H_2O, but consumed to form ROS in the solution following reactions (2)−(4) below:
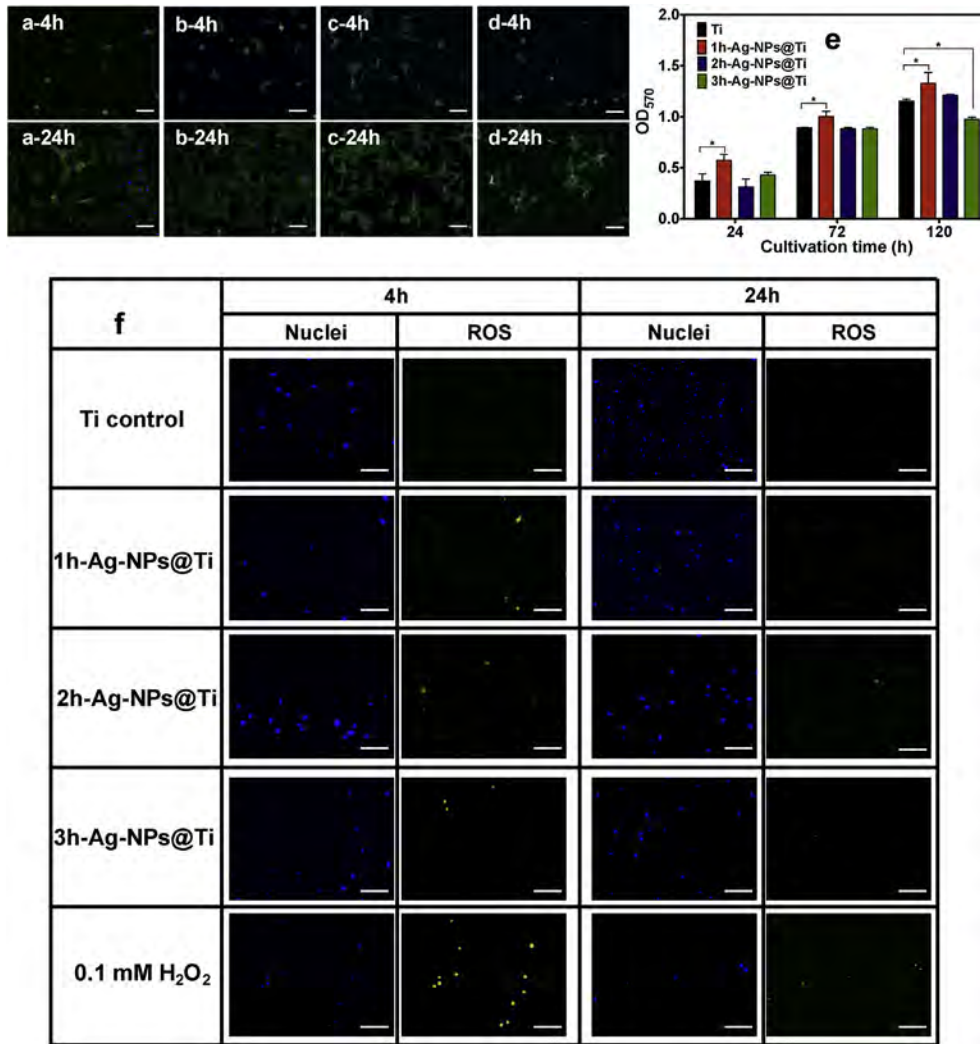
Fig. 7. Cytocompatibility study of samples: (a−d) Cytoskeleton staining of MC3T3-E1 osteoblasts on Ti and Ag-NPs@Ti after culturing for 4 h and 24 h [(a) Ti; (b) 1 h-Ag-NPs@Ti; (c) 2 h-Ag-NPs@Ti; (d) 3 h-Ag-NPs@Ti]. The scale bar is 50 μm. (e) Time-dependent viabilities of MC3T3-E1 osteoblasts by the MTT test after culturing for 1, 3, and 5 days. Significant differences between groups in the OD_{570} values are labeled with * ($p < 0.05$). (f) Fluorescent images of MC3T3-E1 osteoblasts cultured on different samples for 4 h and 24 h stained with DCFH-DA and DAPI. The scale bar is 150 μm.

$$Ti \rightarrow Ti^{n+} + ne^- \qquad (1)$$

$$e^- + O_2 \rightarrow O_2^- \qquad (2)$$

$$2H^+ + O_2^- \rightarrow H_2O_2 \qquad (3)$$

$$O_2 + 2e^- \rightarrow O_2^{2-} \qquad (4)$$

Our data provide direct evidence indicating an antibacterial mechanism based on oxidative stress for Ag-NPs@Ti. Oxidation is considered an important nanoparticle-induced stress which triggers physiological disorder in bacteria [38]. ROS staining and overproduction of superoxide in this work demonstrate an increased endogenous oxidative level [39,40]. Moreover, addition of NAC helps the bacteria defend oxidative stress and so bacteria survive well after NAC addition and the antioxidant test verifies the critical role of oxidative stress in bacteria killing. This over-oxidative environment is responsible for the physiological changes such as depolarization of membrane and protein and DNA/RNA release, which can directly be attributed to the permeability increase of the membrane [41]. Although Ag-NPs can release Ag⁺, which also causes bacteria death, both previous studies [42] and this work show bacteria have very limited exposure to Ag⁺ whose role is thus negligible.

In bacteria, electron transport is a universal behavior in respiration [43]. Electron transfer can also take place when bacteria are in contact with electrically conductive materials [44−46]. In aerobic bacteria, electrons produced by oxidation of compounds for energy production are usually accepted by O_2 which is finally converted to H_2O. It should be noted that electrons to O_2 are not transferred in one step but rather independent steps in which ROS is produced. Normally, the ROS is controlled and consumed sequentially [47]. In the Ag-NPs@Ti systems, the electrons by Ti may go to the intracellular part of the bacteria through the Ag-NPs to disturb the electron transfer process to induce abnormal intracellular production of ROS according to reactions (5)−(7) [48]. These intracellular ROS may work together with the ROS produced in the solution to kill the bacteria. The electron transfer paths and production of in/extra-cellular ROS are schematically illustrated in Fig. 8.
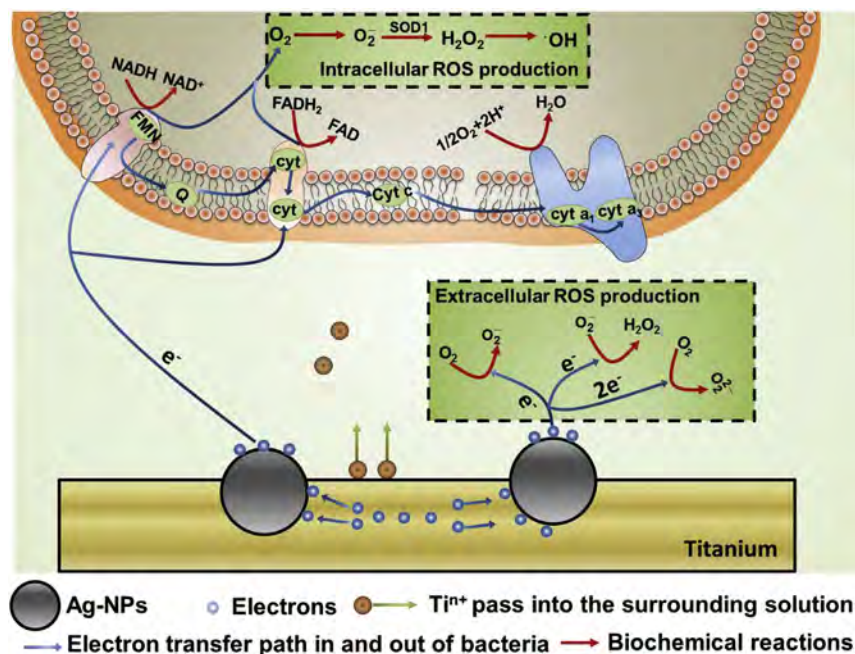
Fig. 8. Generation of oxidative stress in the surrounding solution and within the bacteria.

$$O_2 + e^- \rightarrow O_2^- \tag{5}$$

$$O_2^- \xrightarrow{SOD} H_2O_2 \tag{6}$$

$$H_2O_2 \xrightarrow{Fe^{2+}} \cdot OH \tag{7}$$

5. Conclusion

The antibacterial behavior and underlying mechanism of Ag-NPs@Ti are studied and described. Different from mobile Ag-NPs, the antibacterial effects of Ag-NPs@Ti rely on a conductive substrate. Electrons transfer takes place between the Ag-NPs and Ti substrate and produces ROS in the solution to elevate the oxidative stress at the interface. The electrons can also be transferred to the bacteria to disrupt the respiratory process in the bacteria and produce ROS. The oxidative stress causes physiological changes in the bacteria resulting in bacteria death. Intracellular ROS is also detected from osteoblast cells but it does not affect the cell compatibility. The electron transfer induced oxidative stress described here provides evidence about the antibacterial mechanism of Ag-NPs embedded in Ti and guidance for the design and fabrication of antibacterial materials.

Notes

These authors declare no competing financial interest.

Acknowledgements

Appendix A. Supplementary data

Supplementary data related to this article can be found at http://dx.doi.org/10.1016/j.biomaterials.2017.01.028.

References

[1] M. Geetha, A. Singh, R. Asokamani, A. Gogia, Ti based biomaterials, the ultimate choice for orthopaedic implants—a review, Prog. Mater. Sci. 54 (2009) 397—425.

[2] L. Le Guéhennec, A. Soueidan, P. Layrolle, Y. Amouriq, Surface treatments of titanium dental implants for rapid osseointegration, Dent. Mater 23 (2007) 844—854.

[3] T. Albrektsson, P.-I. Brånemark, H.-A. Hansson, J. Lindström, Osseointegrated titanium implants: requirements for ensuring a long-lasting, direct bone-to-implant anchorage in man, Acta Orthop. Scand. 52 (1981) 155—170.

[4] S. Renvert, A.M. Roos-Jansåker, C. Lindahl, H. Renvert, G. Rutger Persson, Infection at titanium implants with or without a clinical diagnosis of inflammation, Clin. Oral. Implant. Res. 18 (2007) 509—516.

[5] A. Mombelli, M. Oosten, E. Schürch, N. Lang, The microbiota associated with successful or failing osseointegrated titanium implants, Oral Microbiol. Immunol. 2 (1987) 145—151.

[6] M.M. Fürst, G.E. Salvi, N.P. Lang, G.R. Persson, Bacterial colonization immediately after installation on oral titanium implants, Clin. Oral. Implant. Res. 18 (2007) 501—508.

[7] H. Qin, H. Cao, Y. Zhao, C. Zhu, T. Cheng, Q. Wang, et al., In vitro and in vivo anti-biofilm effects of silver nanoparticles immobilized on titanium, Biomaterials 35 (2014) 9114—9125.

[8] H. Cao, X. Liu, F. Meng, P.K. Chu, Biological actions of silver nanoparticles embedded in titanium controlled by micro-galvanic effects, Biomaterials 32 (2011) 693—705.

[9] I. Sondi, B. Salopek-Sondi, Silver nanoparticles as antimicrobial agent: a case study on E. coli as a model for Gram-negative bacteria, J. Colloid Interface Sci. 275 (2004) 177—182.

[10] J.S. Kim, E. Kuk, K.N. Yu, J.-H. Kim, S.J. Park, H.J. Lee, et al., Antimicrobial effects of silver nanoparticles, Nanomed. Nanotechnol. 3 (2007) 95—101.

[11] Q. Feng, J. Wu, G. Chen, F. Cui, T. Kim, J. Kim, A mechanistic study of the antibacterial effect of silver ions on Escherichia coli and Staphylococcus aureus, J. Biomed. Mater. Res. 52 (2000) 662—668.

[12] J.R. Morones, J.L. Elechiguerra, A. Camacho, K. Holt, J.B. Kouri, J.T. Ramírez, et al., The bactericidal effect of silver nanoparticles, Nanotechnology 16 (2005) 2346.

[13] S. Shrivastava, T. Bera, A. Roy, G. Singh, P. Ramachandrarao, D. Dash, Characterization of enhanced antibacterial effects of novel silver nanoparticles, Nanotechnology 18 (2007) 225103.

[14] J.J. Foti, B. Devadoss, J.A. Winkler, J.J. Collins, G.C. Walker, Oxidation of the guanine nucleotide pool underlies cell death by bactericidal antibiotics,

Science 336 (2012) 315–319.

[15] Y. Liu, J.A. Imlay, Cell death from antibiotics without the involvement of reactive oxygen species, Science 339 (2013) 1210–1213.

[16] D.J. Dwyer, P.A. Belenky, J.H. Yang, I.C. MacDonald, J.D. Martell, N. Takahashi, et al., Antibiotics induce redox-related physiological alterations as part of their lethality, Proc. Natl. Acad. Sci. U. S. A. 111 (2014) E2100–E2109.

[17] C. Nathan, A. Cunningham-Bussel, Beyond oxidative stress: an immunologist's guide to reactive oxygen species, Nat. Rev. Immunol. 13 (2013) 349–361.

[18] M.-G. Lee, K.-T. Lee, S.-G. Chi, J.-H. Park, Costunolide induces apoptosis by ROS-mediated mitochondrial permeability transition and cytochrome C release, Biol. Pharm. Bull. 24 (2001) 303–306.

[19] K. Aronsson, U. Rönner, E. Borch, Inactivation of *Escherichia coli, Listeria innocua* and *Saccharomyces cerevisiae* in relation to membrane permeabilization and subsequent leakage of intracellular compounds due to pulsed electric field processing, Int. J. Food Microbiol. 99 (2005) 19–32.

[20] G. Wang, P. Sun, H. Pan, G. Ye, K. Sun, J. Zhang, et al., Inactivation of *Candida albicans* biofilms on polymethyl methacrylate and enhancement of the drug susceptibility by cold Ar/O$_2$ plasma jet, Plasma Chem. Plasma Process 36 (2016) 383–396.

[21] D.J. Novo, N.G. Perlmutter, R.H. Hunt, H.M. Shapiro, Multiparameter flow cytometric analysis of antibiotic effects on membrane potential, membrane permeability, and bacterial counts of *Staphylococcus aureus* and *Micrococcus luteus*, Antimicrob. Agents Chemother. 44 (2000) 827–834.

[22] H. Feng, G. Wang, W. Jin, X. Zhang, Y. Huang, A. Gao, et al., Systematic study of inherent antibacterial properties of magnesium-based biomaterials, ACS Appl. Mater. Interfaces 8 (2016) 9662–9673.

[23] A. Sengupta, U.F. Lichti, B.A. Carlson, A.O. Ryscavage, V.N. Gladyshev, S.H. Yuspa, et al., Selenoproteins are essential for proper keratinocyte function and skin development, PLoS One 5 (2010) e12249.

[24] S.B. Amor, G. Baud, M. Jacquet, G. Nanse, P. Fioux, M. Nardin, XPS characterisation of plasma-treated and alumina-coated PMMA, Appl. Surf. Sci. 153 (2000) 172–183.

[25] G.D. Shockman, J. Barren, Structure, function, and assembly of cell walls of gram-positive bacteria, Annu. Rev. Microbiol. 37 (1983) 501–527.

[26] Y. Zhao, H. Cao, H. Qin, T. Cheng, S. Qian, M. Cheng, et al., Balancing the osteogenic and antibacterial properties of titanium by codoping of Mg and Ag: an *in vitro* and *in vivo* study, ACS Appl. Mater. Interfaces 7 (2015) 17826–17836.

[27] A. Medveďová, Ľ. Valík, Staphylococcus aureus: characterisation and quantitative growth description in milk and artisanal raw milk cheese production, Structure and function of food engineering, Rij. InTech (2012) 71–102.

[28] I. Sur, D. Cam, M. Kahraman, A. Baysal, M. Culha, Interaction of multifunctional silver nanoparticles with living cells, Nanotechnology 21 (2010) 175104.

[29] R. Barrena, E. Casals, J. Colón, X. Font, A. Sánchez, V. Puntes, Evaluation of the ecotoxicity of model nanoparticles, Chemosphere 75 (2009) 850–857.

[30] S. Pal, Y.K. Tak, J.M. Song, Does the antibacterial activity of silver nanoparticles depend on the shape of the nanoparticle? A study of the gram-negative bacterium *Escherichia coli*, Appl. Environ. Microbiol. 73 (2007) 1712–1720.

[31] H. Cao, Y. Qiao, X. Liu, T. Lu, T. Cui, F. Meng, et al., Electron storage mediated dark antibacterial action of bound silver nanoparticles: smaller is not always better, Acta Biomater. 9 (2013) 5100–5110.

[32] V.K. Truong, R. Lapovok, Y.S. Estrin, S. Rundell, J.Y. Wang, C.J. Fluke, et al., The influence of nano-scale surface roughness on bacterial adhesion to ultrafine-grained titanium, Biomaterials 31 (2010) 3674–3683.

[33] A.V. Singh, V. Vyas, R. Patil, V. Sharma, P.E. Scopelliti, G. Bongiorno, et al., Quantitative characterization of the influence of the nanoscale morphology of nanostructured surfaces on bacterial adhesion and biofilm formation, PLoS One 6 (2011) e25029.

[34] J. Li, G. Wang, H. Zhu, M. Zhang, X. Zheng, Z. Di, et al., Antibacterial activity of large-area monolayer graphene film manipulated by charge transfer, Sci. Rep. 4 (2014) 4359.

[35] P. Vanýsek, Electrochemical Series, CRC Press LLC, 2000.

[36] M.O. Clements, S.J. Foster, Stress resistance in *Staphylococcus aureus*, Trends Microbiol. 7 (1999) 458–462.

[37] M.O. Clements, S.P. Watson, S.J. Foster, Characterization of the major superoxide dismutase of *Staphylococcus aureus* and its role in starvation survival, stress resistance, and pathogenicity, J. Bacteriol. 181 (1999) 3898–3903.

[38] M.J. Hajipour, K.M. Fromm, A.A. Ashkarran, D.J. de Aberasturi, I.R. de Larramendi, T. Rojo, et al., Antibacterial properties of nanoparticles, Trends Biotechnol. 30 (2012) 499–511.

[39] X. Chen, X. Huang, C. Zheng, Y. Liu, T. Xu, J. Liu, Preparation of different sized nano-silver loaded on functionalized graphene oxide with highly effective antibacterial properties, J. Mater. Chem. B 3 (2015) 7020–7029.

[40] E. Cabiscol, J. Tamarit, J. Ros, Oxidative stress in bacteria and protein damage by reactive oxygen species, Int. Microbiol. 3 (2010) 3–8.

[41] O. Blokhina, E. Virolainen, K.V. Fagerstedt, Antioxidants, oxidative damage and oxygen deprivation stress: a review, Ann. Bot. 91 (2003) 179–194.

[42] S. Kim, J.E. Choi, J. Choi, K.-H. Chung, K. Park, J. Yi, et al., Oxidative stress-dependent toxicity of silver nanoparticles in human hepatoma cells, Toxicol. Vitro 23 (2009) 1076–1084.

[43] M. Okamura, M. Paddock, M. Graige, G. Feher, Proton and electron transfer in bacterial reaction centers, Biochim. Biophys. Acta, Bioenerg. 1458 (2000) 148–163.

[44] E. Dumas, C. Gao, D. Suffern, S.E. Bradforth, N.M. Dimitrijevic, J.L. Nadeau, Interfacial charge transfer between CdTe quantum dots and gram negative vs gram positive bacteria, Environ. Sci. Technol. 44 (2010) 1464–1470.

[45] V. Nadtochenko, N. Denisov, O. Sarkisov, D. Gumy, C. Pulgarin, J. Kiwi, Laser kinetic spectroscopy of the interfacial charge transfer between membrane cell walls of *E. coli* and TiO$_2$, J. Photochem. Photobiol. A 181 (2006) 401–407.

[46] G. Wang, H. Feng, A. Gao, Q. Hao, W. Jin, X. Peng, et al., Extracellular electron transfer from aerobic bacteria to Au-loaded TiO$_2$ semiconductor without light: a new bacteria-killing mechanism other than localized surface plasmon resonance or microbial fuel cells, ACS Appl. Mater. Interfaces 8 (2016) 24509–24516.

[47] J.F. Turrens, Reactive Oxygen Species, Encyclopedia of Biophysics, Springer, 2013, pp. 2198–2200.

[48] M. Giorgio, E. Migliaccio, F. Orsini, D. Paolucci, M. Moroni, C. Contursi, et al., Electron transfer between cytochrome c and p66 Shc generates reactive oxygen species that trigger mitochondrial apoptosis, Cell 122 (2005) 221–233.

Supplementary Information

Antibacterial Effects of Titanium Embedded with Silver Nanoparticles Based on Electron-Transfer-Induced Reactive Oxygen Species

Guomin Wang[1], Weihong Jin[1], Abdul Mateen Qasim[1], Ang Gao[1], Xiang Peng[1], Wan Li[1], Hongqing Feng[1,2,*], Paul K. Chu[1,*]

[1] Department of Physics and Materials Science, City University of Hong Kong, Tat Chee Avenue, Kowloon, Hong Kong, China

[2] Beijing Institute of Nanoenergy and Nanosystems, Chinese Academy of Sciences; National Center for Nanoscience and Technology (NCNST), Beijing 100083, P. R. China

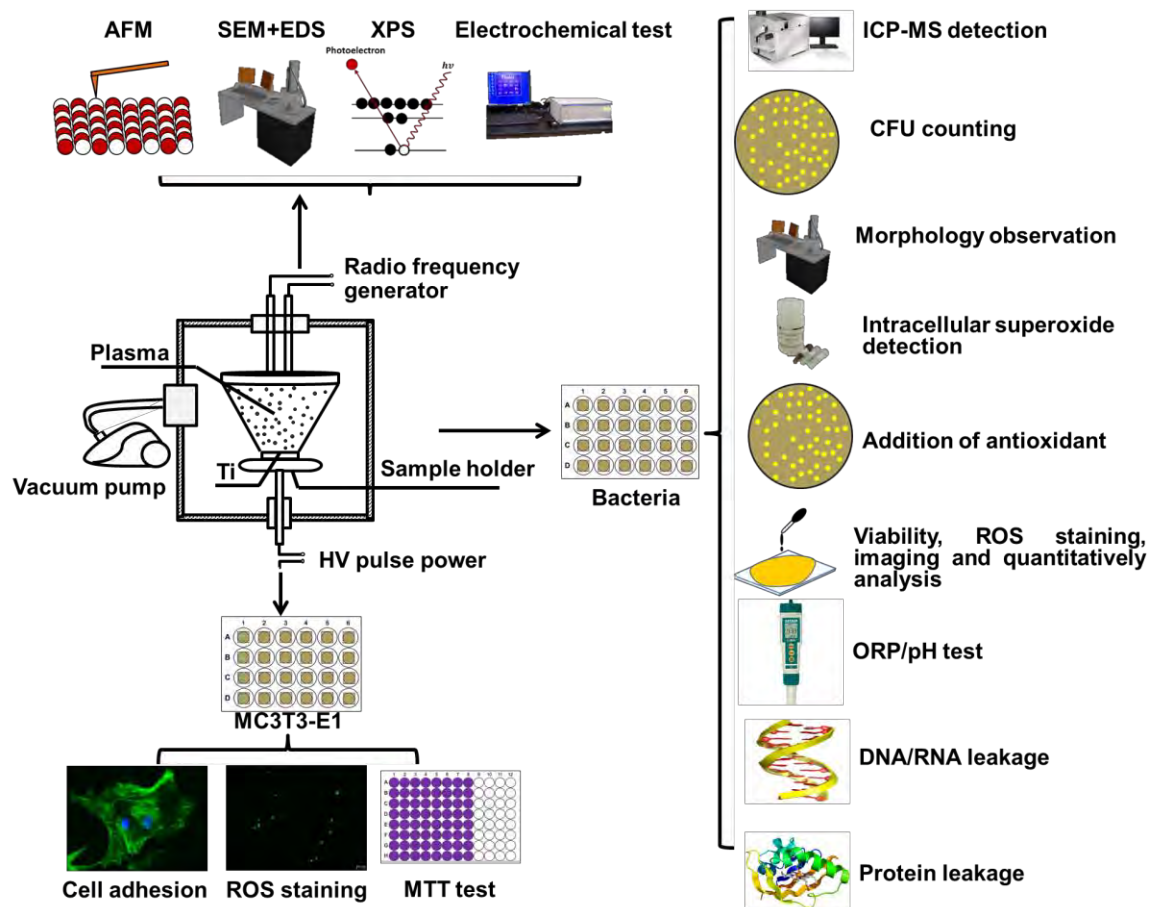# 1. Materials and methods

1.1. Experimental procedures

Figure S1. Schematic illustration of the experimental protocols including sample preparation, characterization, antibacterial effect assay, physiological study of bacteria, and biocompatibility test.

1.2. Morphology characterization

Scanning electron microscopy (SEM, JSM-820, JEOL Ltd., Japan) was used to examine the morphology of the bacteria. The samples with adhered bacteria were collected at different time points, fixed with 2.5% glutaraldehyde overnight, dehydrated with ethanol with concentrations of 10%, 30%, 50%, 70%, 90%, and 100% sequentially, and dried in vacuum prior to examination by SEM.
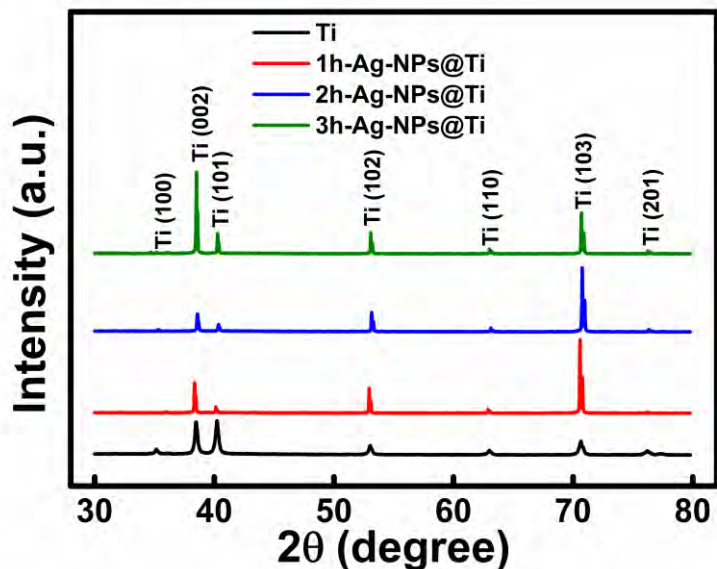
2. Results

2.1. Surface characterization.

Fig. S2. XRD spectra of the samples.

2.1. Bacteria morphology

SEM is conducted to observe the morphology of the bacteria after culturing for different time periods (**Figure S3)**. Ti provides a friendly environment for *S. aureus* and a mature biofilm forms on the Ti plate after 24 h [**Figure S3**(a)]. Compared to the Ti group, fewer bacteria adhere onto the surface of the Ag-NPs@Ti groups and the bacteria fail to form a biofilm on them [**Figure S3** (b-d)]. This is consistent with the antibacterial effects. These results combined with the data on the antibacterial rates verify the inhibition effects of Ag-NPs@Ti during the *S. aureus* biofilm formation process.
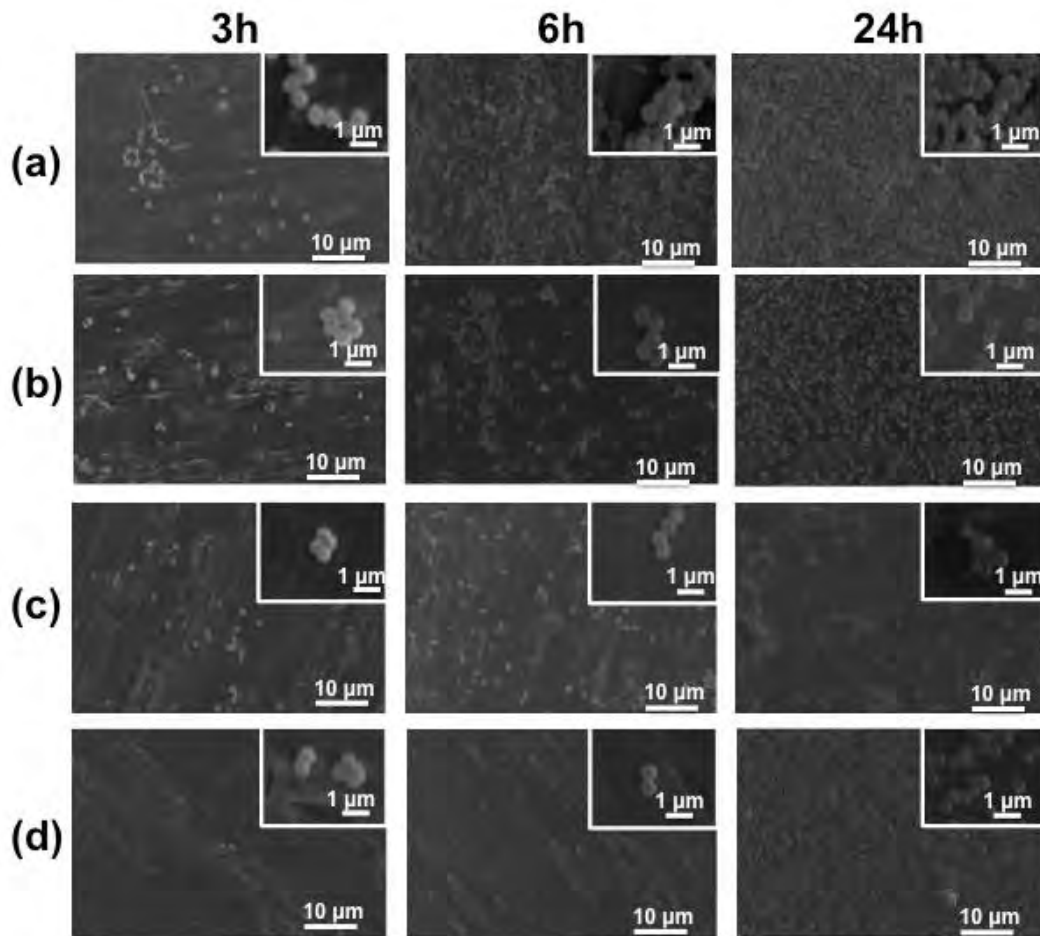

Figure S3. SEM images of *S. aureus* cultivated on (a) Ti, (b) 1h-Ag-NPs@Ti, (c) 2h-Ag-NPs@Ti, and (d) 3h-Ag-NPs@ Ti for different time periods.